Compensation of Oxygen Doping in p-Type Organic Field-Effect Transistors Utilizing Immobilized n-Dopants

Marc-Michael Barf,* Frank S. Benneckendorf, Patrick Reiser, Rainer Bäuerle, Wolfgang Köntges, Lars Müller, Martin Pfannmöller, Sebastian Beck, Eric Mankel, Jan Freudenberg, Daniel Jänsch, Jean-Nicolas Tisserant, Robert Lovrincic, Rasmus R. Schröder, Uwe H. F. Bunz, Annemarie Pucci, Wolfram Jaegermann, Wolfgang Kowalsky,* and Klaus Müllen*

Poly(3-hexyl-thiophene-2,5-diyl) (P3HT) is one of the most commonly used materials in organic electronics, yet it is considered to be rather unattractive for organic field-effect transistors (OFETs) due to its tendency to oxidize under aerobic conditions. Strong p-doping of P3HT by oxygen causes high off-currents in such devices opposing the desired high on/off-ratios. Herein, a new application-oriented method involving the recently developed immobilizable organic n-dopant 2-(2-((4-azidobenzyl)oxy)phenyl)-1,3-dimethyl-2,3-dihydro-1H-benzoimidazol (o-AzBnO-DMBI) is presented allowing to process and operate P3HT OFETs in air. The n-dopants compensate oxygen doping by trapping generated free holes, thereby rediminishing OFET off-currents by approximately two orders of magnitude. At the same time, field-effect mobilities remain high in the order of up to 0.19 cm^2 V^{-1} s^{-1}. Due to the covalent attachment of the dopants to the host matrix after photochemical activation, a drift of the otherwise mobile ions within the device is prevented even at high operating voltages and, thus, hysteresis in the corresponding transfer characteristics is kept low. In this manner, the air instability of P3HT OFETs is successfully resolved paving an auspicious way toward OFET mass production. As the immobilization process employed here is nonspecific with respect to the host material, this strategy is transferable to other p-type semiconductors.

1. Introduction

Low cost processing makes organic semiconductors an interesting candidate in current research and development of electronic applications. One of the very extensively applied materials, especially in the field of organic solar cells, is the conjugated polymer poly(3-hexyl-thiophene-2,5-diyl) (P3HT).[1–4] This widely commercially available material can be synthesized on large scales and with high reproducibility via controlled methods.[5–7] Manufacturing processes involving P3HT have been well investigated leading to large scale, fully roll-to-roll printed solar modules.[8–10] For these reasons, P3HT seems like a highly promising candidate for mass production of electronic devices. Other than in organic solar cells however, it is used only rather sporadically in organic field-effect transistors (OFETs) up to date. This originates from the polymer's instability with respect to oxygen, the latter infiltrating the

Dr. M.-M. Barf, Dr. L. Müller, Dr. J.-N. Tisserant, Dr. R. Lovrincic,
Prof. W. Kowalsky
Institute for High Frequency Technology
Technical University of Braunschweig
Schleinitzstraße 22, Braunschweig 38106, Germany
E-mail: m.barf@tu-braunschweig.de; wolfgang.kowalsky@ihf.tu-bs.de
Dr. M.-M. Barf, Dr. F. S. Benneckendorf, Dr. P. Reiser, R. Bäuerle,
Dr. L. Müller, Dr. S. Beck, Dr. E. Mankel, Dr. J. Freudenberg, D. Jänsch,
Dr. J.-N. Tisserant, Dr. R. Lovrincic, Prof. U. H. F. Bunz, Prof. A. Pucci,
Prof. W. Jaegermann, Prof. W. Kowalsky, Prof. K. Müllen
InnovationLab
Speyerer Straße 4, Heidelberg 69115, Germany
E-mail: muellen@mpip-mainz.mpg.de

The ORCID identification number(s) for the author(s) of this article can be found under https://doi.org/10.1002/admt.202000556.

Dr. F. S. Benneckendorf, Dr. J. Freudenberg, D. Jänsch, Prof. U. H. F. Bunz
Institute of Organic Chemistry
Heidelberg University
Im Neuenheimer Feld 270, Heidelberg 69120, Germany
Dr. P. Reiser, Dr. E. Mankel, Prof. W. Jaegermann
Materials Science Department
Surface Science Division
Technical University of Darmstadt
Otto-Berndt-Straße 3, Darmstadt 64287, Germany
R. Bäuerle, Dr. L. Müller, Dr. S. Beck, Prof. A. Pucci, Prof. W. Kowalsky
Kirchhoff Institute for Physics
Heidelberg University
Im Neuenheimer Feld 227, Heidelberg 69120, Germany
W. Köntges, Dr. M. Pfannmöller, Prof. A. Pucci
Centre for Advanced Materials
Heidelberg University
Im Neuenheimer Feld 225, Heidelberg 69120, Germany

**ADVANCED
SCIENCE NEWS**
www.advancedsciencenews.com

**ADVANCED
MATERIALS
TECHNOLOGIES**
www.advmattechnol.de

organic thin film and creating reversible P3HT–O_2 adducts.[11,12] These can trap photogenerated electrons and form charge-transfer-complexes inducing p-doping in the polymer.[11] In the dark, p-doping is explained by physical adsorption of the oxygen on the polymer affecting the energetic structure rather than by a photochemical reaction.[13] Meijer et al. have shown that air exposure in the dark strongly increases OFET off-currents due to p-doping of the P3HT bulk.[14] They furthermore reveal that this doping process is reversible in vacuum, which is decreasing the off-currents again. Another option to reduce off-currents is compensation doping, which also works under ambient conditions.[15] p-Doping can be compensated by the insertion of n-dopants, which localize free holes in the semiconductor and, thus, reduce free charge carrier density. This method is particularly common in inorganic electronics.[16–20] Due to high doping efficiencies compared to organic electronics, it is possible to use low doping concentrations for this purpose,[21,22] which are less likely to affect the semiconductor in its morphology. Contrarily, organic electronics typically require significantly higher doping concentrations.[23,24]

In order to achieve lasting high on/off-ratios in air, Lu et al. used blends of P3HT and polystyrene doped with the p-dopant tetrafluoro-tetracyanoquinodimethane (F$_4$TCNQ).[25] Blends between two polymers in OFETs are often capable to improve certain device properties.[25–28] However, the drift observable for dopants such as F$_4$TCNQ as well as molybdenum tris[1-(methoxycarbonyl)-2-(trifluoromethyl)-ethane-1,2-dithiolene] (Mo(tfd-CO$_2$Me)$_3$)) in P3HT does strongly impacts the polymer's electronic properties and thus device stability.[29,30] When blending the n-dopant 2-(2-methoxyphenyl)-1,3-dimethyl-2,3-dihydro-1H-benzoimidazole (o-MeO-DMBI) with P3HT films, Lee et al. observed a reduction of off-currents in air at the prize of a strong hysteresis in OFET transfer characteristics, which they then used to add a memristive component to their devices.[15] Although there are other examples of intentionally using hysteresis effects for memristive applications, they are usually not desired for normal operation.[29,31–33] This behavior suggests that such n-dopants are also prone to drift phenomena in P3HT, which are detrimental for sole OFET performance. Dopants and self-assembled monolayers (SAMs) are a well-known tool to influence morphology and device parameters but which can be disadvantageous when migrating through the organic host in operation.[34–37] Hence, inhibiting dopant migration to achieve stable device operation is of great importance. 1,3-dimethyl-2-phenyl-2,3-dihydro-1H-benzoimidazole (DMBI) derivatives are solution-processable and air-stable n-dopants, which have so far mostly been used to efficiently dope 6,6-phenyl-C$_{61}$-butyric acid methyl ester (PCBM) or n-type polymers.[38–42] For PCBM, the increase in conductivity appears to be even larger than for polymers, which is presumably due
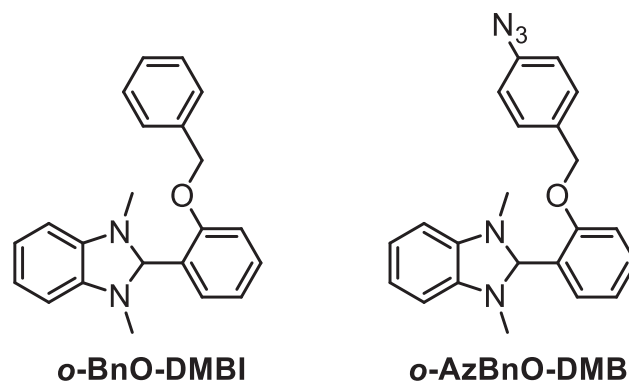

Figure 1. Chemical structures of o-BnO-DMBI (left) and o-AzBnO-DMBI (right).

to the better miscibility of such dopants and fullerenes in comparison.[38,43,44] The doping mechanism itself is still open to debate, but has been investigated for the case of PCBM multiple times suggesting either a hydride transfer to the host or a hydrogen radical transfer with a subsequent electron transfer, which would both lead to a generation of cationic DMBI as well as PCBM radical anions.[39,40,45]

We recently reported the covalent attachment of an azide-functionalized DMBI derivative to PCBM leading to its immobilization in this host matrix.[46] 2-(2-((4-Azidobenzyl)oxy)phenyl)-1,3-dimethyl-2,3-dihydro-1H-benzoimidazol (o-AzBnO-DMBI) was compared to its nonfunctionalized counterpart 2-(2-(benzyloxy)phenyl)-1,3-dimethyl-2,3-dihydro-1H-benzoimidazole (o-BnO-DMBI) shown in **Figure 1**. o-AzBnO-DMBI exhibits a comparable doping strength, while it covalently binds to PCBM after activation through deep ultraviolet light (UV, 254 nm) resulting in the dopant's immobilization within the host matrix. The applied immobilization strategy via nitrene generation is thereby nonspecific to the host molecule and hence could be used to also suppress the dopant drift in P3HT films as investigated in this work. Scanning and transmission electron microscopy (SEM and TEM) show similar distributions of both o-AzBnO-DMBI and the nonfunctionalized o-BnO-DMBI in P3HT films. Infrared (IR) spectroscopy is used to analyze the binding process between o-AzBnO-DMBI and P3HT and photoelectron spectroscopy reveals the energy level shifts through doping, before the doped films are integrated in OFETs processed and operated in air. We show that although both dopants increase the on/off-ratio of the devices through decreasing off-currents, the transistors with o-BnO-DMBI exhibit a strong hysteresis during device operation as well as significantly lower field-effect mobilities, while transistors with the immobilized o-AzBnO-DMBI are hysteresis-free due to the suppression of the drift of the immobilized dopants within the P3HT matrix.

2. Results and Discussion

P3HT was doped with o-BnO-DMBI and o-AzBnO-DMBI via solution mixing using chlorobenzene as a solvent before spin-coating the blend. Maximum doping efficiency is reported for DMBI doped thin films after an annealing temperature of 75 °C.[40] Undoped P3HT sandwiched between gold contacts
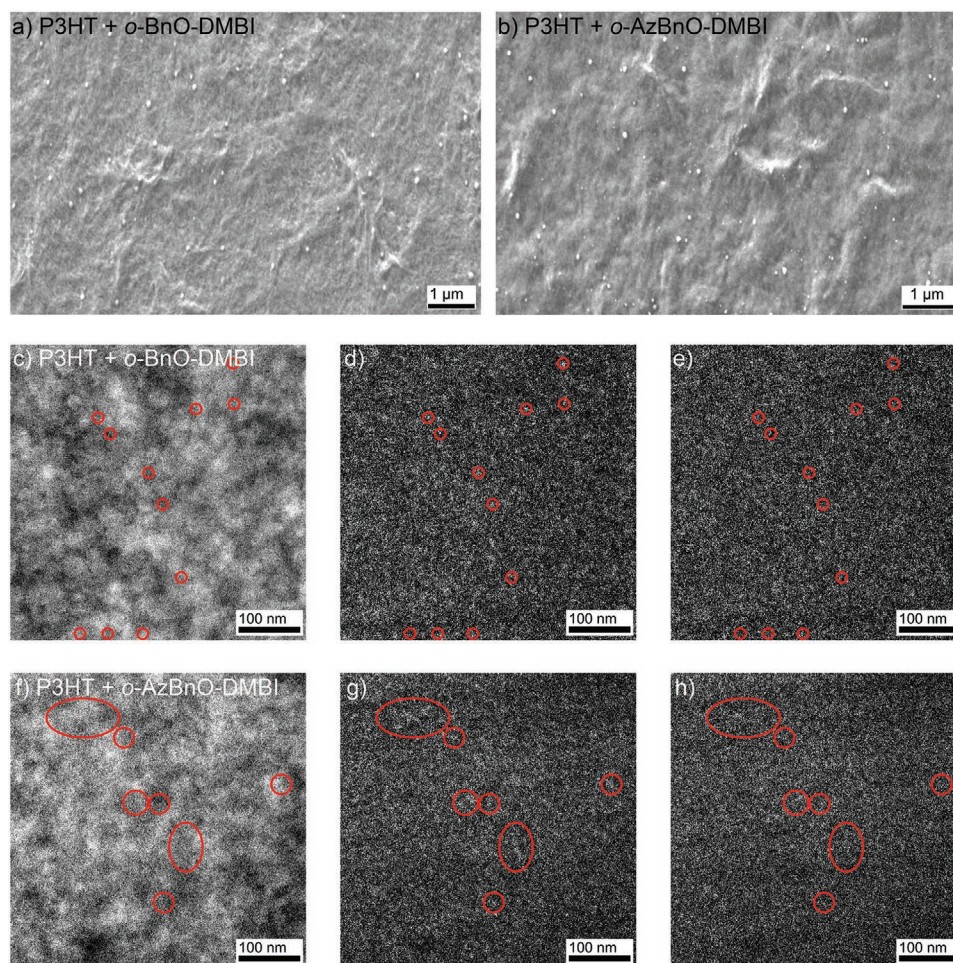
Prof. R. R. Schröder
3DMM2O
Cluster of Excellence (EXC-2082/1 - 390761711) and CAM - Centre for Advanced Materials
Heidelberg University
Heidelberg 69120, Germany

Prof. K. Müllen
Max Planck Institute for Polymer Research
Ackermannweg 10, Mainz 55128, Germany

ADVANCED
SCIENCE NEWS
www.advancedsciencenews.com

ADVANCED
MATERIALS
TECHNOLOGIES
www.advmattechnol.de

Figure 2. Distribution of *o*-BnO-DMBI and *o*-AzBnO-DMBI in the P3HT matrix. SEM images of a) *o*-BnO-DMBI and b) *o*-AzBnO-DMBI in P3HT films. Visualization of c–e) *o*-BnO-DMBI and f–h) *o*-AzBnO-DMBI in P3HT films at the nanoscale using electron spectroscopic imaging (ESI) in the transmission electron microscope (TEM). c,f) Conventional TEM images show no material contrast between dopant and P3HT. d,g) ESI images at 6.5 eV show specific material contrast due to differences in plasmon excitations of π-electrons. Red circles mark several positions of areas with elevated π-electron excitation signal, i.e., areas containing dopant agglomerates. For second exposures to generate e,h) 6.5 eV ESI images, the dopant signal disappears due to irradiation damage. All films contain 10 mol% of dopant in the blend.

as in an OFET-architecture holds conductivities in the range of 10^{-2} S m^{-1} obtained by *IV*-measurements in air. During such processing and characterizing samples usually were under direct air influence for ≈3 h. The high intrinsic conductivity stemming from p-doping through air oxygen is exceedingly obstructive for OFET performance. With 10 mol% of *o*-BnO-DMBI blended in the P3HT the film, conductivity is reduced drastically through compensation doping by four orders of magnitude to ≈10^{-6} S m^{-1} allowing lower off-currents in transistors operated in air. Annealing the films at 75 °C decreases the conductivity even further, which is not significantly affected by UV treatment. For the immobilizable dopant *o*-AzBnO-DMBI a similar behavior is found (Figure S1, Supporting Information). Besides the changes in conductivity, this n-dopant can be detected in UV–vis spectra of doped films as well, since the azide functional group absorbs light at around 250 nm. Therefore, the spectra of P3HT films doped with *o*-AzBnO-DMBI feature a higher absorptivity at this wavelength compared to undoped P3HT films or films doped with *o*-BnO-DMBI (Figure S2, Supporting Information).

SEM reveals dopant agglomerates with sizes in the order of 100 nm at the surface of the films for both species (**Figure 2**a,b). Such large dopant clusters could derive from a nonoptimal miscibility of the dopant and the polymer and have already been reported for similar systems.[44] Due to phase segregation the dopants could potentially demix from the wet film during processing, where they then aggregate on the surface. Dopant distributions inside the P3HT films can be visualized using electron spectroscopic imaging (ESI) in the transmission electron microscope. The contrast in conventional bright-field images is primarily determined by mass–thickness variations (Figure 2c,d). The high carbon content and similar elemental composition of both materials do not allow to differentiate between them in a blend system. By applying low-energy loss ESI, varying absorption properties of the dopants and P3HT can be used for determining the material distribution at the nanometer scale.[47] The principal differences between optical excitation signals between P3HT and the dopants *o*-BnO-DMBI and *o*-AzBnO-DMBI are shown in electron energy loss spectroscopy (EELS) (Figure S3, Supporting Information). In the EEL spectra,
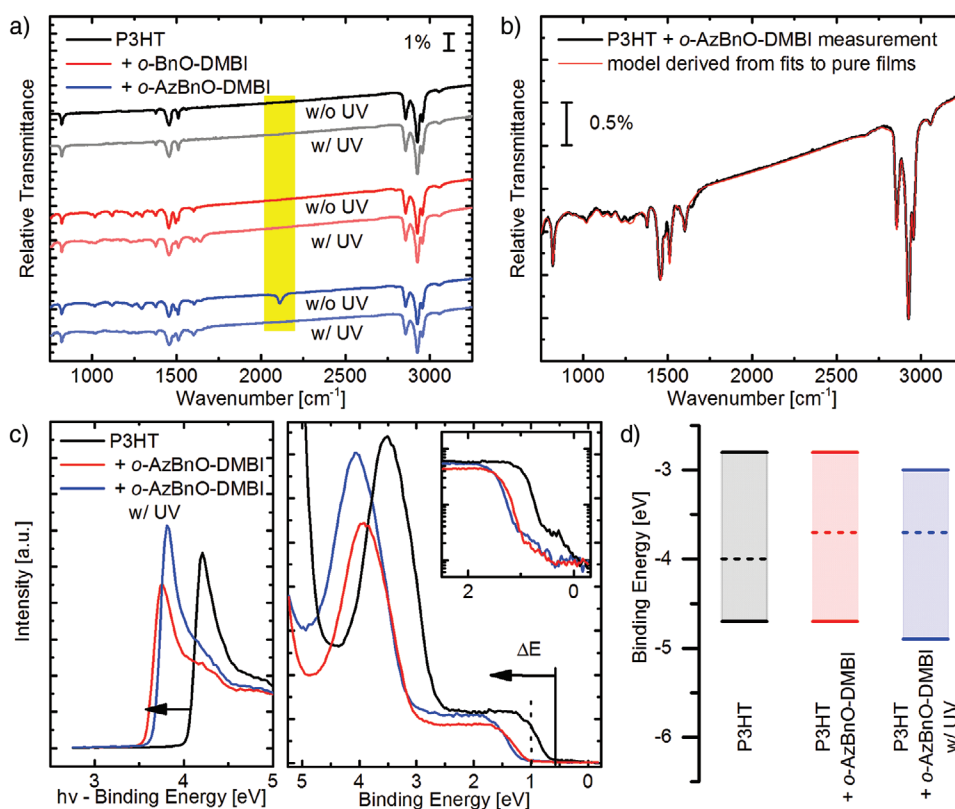
**ADVANCED
SCIENCE NEWS**

www.advancedsciencenews.com

**ADVANCED
MATERIALS
TECHNOLOGIES**

www.advmattechnol.de

Figure 3. IR spectroscopy and photoelectron spectroscopy on DMBI-doped P3HT films. a) IR spectra of thin films with pure P3HT as well as P3HT doped with o-BnO-DMBI and o-AzBnO-DMBI, respectively. Each film was measured before and immediately after a 15 min UV treatment. The anchor group creates an absorption peak at around 2100 cm⁻¹ that can only be seen before UV treatment. b) Measurement and fit of IR spectra of P3HT with o-AzBnO-DMBI after UV treatment. The fit results from a layer stack of fits to pure UV activated o-AzBnO-DMBI on top of pure UV treated P3HT. c) HOMO of P3HT blended with o-AzBnO-DMBI measured by UPS together with the secondary electron cutoff recorded with XPS. A semilog plot of the onset region is given as an inset. d) A schematic band diagram of air-exposed undoped P3HT as well as doped P3HT is derived from the measurements assuming a constant bandgap of $E_g = 1.9$ eV. All films contain 10 mol% of dopant in the blend.

both dopants exhibit a strong energy loss signal at 6.5 eV, which disappears after applying a specific electron dose due to irradiation damage. The polymer does not show a pronounced peak at this energy loss value indicating less excitation of π-electrons. Hence, when performing ESI at this energy loss, a dopant agglomerate would appear bright on dark background. For both dopants bright areas of 5–10 nm in size appear in a 6.5 eV ESI image on undamaged areas (Figure 2d,g). The agglomerates visualized in the ESI images are homogeneously distributed, but reveal that dopants do not show molecular dispersion in P3HT. The contrasts attributed to dopant agglomerates disappear after a second exposure while recording 6.5 eV ESI images of identical areas because of irradiation damage (Figure 2e,h). This proofs that in the first exposure, dopants are visualized due to the elevated excitation of π-electrons. For more information, we refer to the Supporting Information and Pfannmöller et al.[47]

To further investigate the interaction between host polymer and the dopants, films with pure P3HT and blends with either o-BnO-DMBI or o-AzBnO-DMBI were analyzed with IR spectroscopy as well as X-ray photoelectron spectroscopy (XPS) and ultraviolet photoelectron spectroscopy (UPS) as shown in **Figure 3**. For pure P3HT and P3HT doped with 10 mol% o-BnO-DMBI, only marginal changes in the IR spectra were observed after a UV treatment of the films. All absorption peaks

of P3HT are present in the blends for both dopant species. The only notable difference in the spectra is the absorption peak of the azide at around 2100 cm⁻¹ in case of doping with o-AzBnO-DMBI, which vanishes after UV treatment pointing toward a successful anchoring of the dopant (Figure 3a). Thus, the reactive azide does not decompose or significantly alter the polymer backbone after photochemical activation. For a better identification of the influence of o-AzBnO-DMBI on P3HT, a layer stack with pure UV activated o-AzBnO-DMBI on top of pure UV treated P3HT was simulated with the total thickness fitted to the experimental data of a UV treated blend of both materials (Figure 3b). The fitting of the thickness only serves for better comparability without altering the validity of the data. The comparison between simulation and measurement allows for speculation about the binding mechanism between o-AzBnO-DMBI and P3HT. If the dopant binds to the polymer-backbone, the intensity of C–H vibrations at around 820 cm⁻¹ should clearly decrease. If it binds to the sidechains, only one of five identical CH₂ vibrations of the corresponding P3HT monomer should be affected resulting in at the most marginal changes of the absorption overall. Since there is no considerable difference between the simulation and the measurement, we assume that the azide rather binds to the P3HT side chains than to the polymer-backbone. In fact, the lack of difference over the entire IR
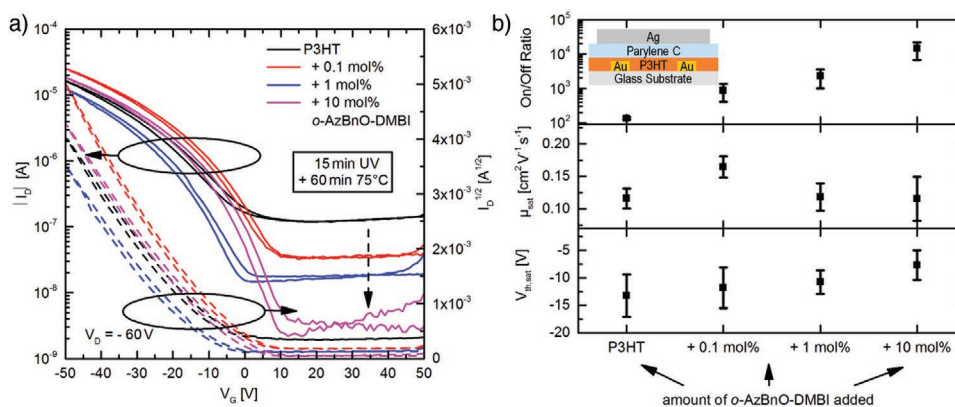
ADVANCED
SCIENCE NEWS
www.advancedsciencenews.com

ADVANCED
MATERIALS
TECHNOLOGIES
www.advmattechnol.de

Figure 4. OFETs with immobilized o-AzBnO-DMBI processed and operated in air. a) Increasing the content of o-AzBnO-DMBI in P3HT films leads to a continuous reduction in OFET off-currents. Films were treated with UV light for 15 min before heating them at 75 °C for 1 h. Shown are the devices with highest field-effect mobility, respectively. b) The reduction in off-currents through compensation doping leads to increasing on–off ratios with higher dopant content, while mobilities in the saturation regime remain high and threshold voltages slightly improve.

spectrum additionally verifies the integrity of both materials in the blend after UV treatment. Eventually, the possibility for the dopants to bind to each other cannot be eliminated potentially facilitated by the agglomerate formation observed.

A decrease in film conductivity attributed to compensation doping requires a reduction of the free charge carrier concentration, likely accompanied by a Fermi-level shift from a p-type position toward the center of the bandgap. Although measured in vacuum, this is observed for the XPS/UPS spectra of the n-doped P3HT films, where the highest occupied molecular orbital (HOMO) onset is shifted toward higher binding energies compared to air-processed P3HT (Figure 3c). The same shift can also be traced in all XPS core-level spectra. Furthermore, the N 1s emission reveals the cationic DMBI species in the P3HT blend confirming an efficient redox reaction with the host (Figure S4, Supporting Information). To exclude charging effects, which can occur at higher film resistivity, several control and comparative experiments were conducted, suggesting that the observed Fermi-level shift is indeed due to compensation of p-doping or filling of bandgap states. From this shift, the corresponding band diagram can be concluded (Figure 3d). The ionization potential is derived from the measured work function, to which the HOMO onset is added. The electron affinity is then estimated via an approximate constant bandgap of 1.9 eV. A slight shift of the HOMO position with respect to the vacuum level after UV activation could be caused by small variations of the surface dipole.

When integrated in OFETs fabricated and operated in air, o-AzBnO-DMBI first of all leads to the desired decrease in off-currents. In oxygen-doped P3HT, off-currents above 10^{-7} A are observed. Through compensation doping with o-AzBnO-DMBI, these can continuously be decreased with increasing dopant content to almost 10^{-9} A for a final ratio of 10 mol%, which consequently results in an increase of on/off-ratios in OFET transfer curves by two orders of magnitude as shown in **Figure 4**. The compensation doping also reflects in a current reduction in the output curves, where devices with o-AzBnO-DMBI moreover show a distinctly better saturation of the currents for higher operating voltages (Figure S5, Supporting Information). Overall, the reduction in currents can directly be correlated to a reduction in conductivity of the films (Figure S6,

Supporting Information). Already very small ratios such as 0.1 mol% lead to a decrease in film conductivity by approximately two orders of magnitude causing a corresponding reduction in OFET off-currents. Such low concentrations furthermore even seem to slightly increase the field-effect mobility of the transistors to 0.19 cm² V⁻¹ s⁻¹ for the best device. This is especially promising concerning the transfer of this compensation doping approach to other host systems, which potentially exhibit an even better miscibility with the dopant and thus a better doping efficiency, so that lower amounts of the dopant could already be sufficient. On the other hand, the field-effect mobilities of the P3HT devices shown here also remain high in the range of 0.1 cm² V⁻¹ s⁻¹ with a considerably large dopant content of 10 mol%.

The average threshold voltages of the OFETs slightly improve with an increasing amount of dopants in the P3HT films. While transistors with undoped P3HT films exhibit a threshold voltage of ≈-13 V, this value changes to less than -8 V in average for a ratio of 10 mol% o-AzBnO-DMBI. n-Type doping typically leads to a shift of threshold voltages even further into the negative regime.[36,48,49] However, compensation doping decreases the free charge carrier concentration, but unlike normal doping, leaves the overall charge carrier density unchanged.[24] A shift to smaller absolute threshold voltages is explicable with the observed dopant agglomerates. Especially with large amounts of o-AzBnO-DMBI in the thin film, dopants bound to each other after UV activation instead of the P3HT matrix can potentially form mobile and charged clusters. These can then migrate within the film during device operation changing its electrical properties and affecting the threshold voltage.

The drifting mechanism becomes even more evident when looking at the nonfunctionalized dopant o-BnO-DMBI or not UV activated o-AzBnO-DMBI. Missing the azide unit, o-BnO-DMBI cannot be immobilized through UV treatment, which again is mandatory for the immobilization of o-AzBnO-DMBI in and covalent attachment to the P3HT matrix. Heat treatment alone is not sufficient either for this dopant. In all these cases, the transfer curves of the corresponding OFETs show a strong hysteresis and notably inferior field-effect mobilities as can be seen in **Figure 5**. The hysteresis is related to a shift of threshold voltages measured in the forward direction toward the positive

**ADVANCED
SCIENCE NEWS**

www.advancedsciencenews.com

**ADVANCED
MATERIALS
TECHNOLOGIES**

www.advmattechnol.de

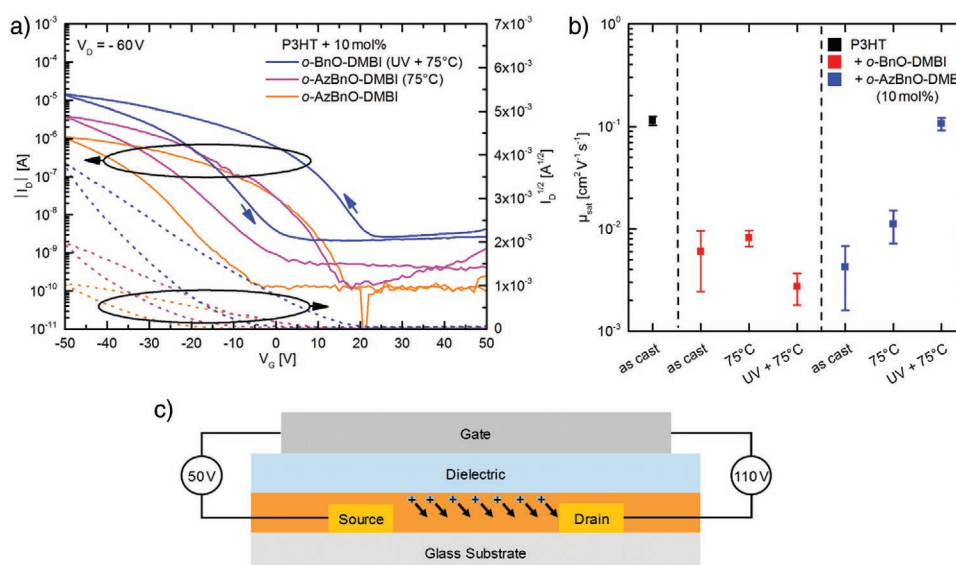**Figure 5.** OFETs with nonimmobilized n-dopants processed and operated in air. a) o-BnO-DMBI and not UV activated o-AzBnO-DMBI cause strong hysteresis in P3HT OFETs due to dopant drift. b) This also reflects on the field-effect mobilities of the devices. Not immobilized dopants lead to a decrease in mobility by at least one order of magnitude. c) The setting at the beginning of transfer characteristic measurement with the source voltage at 0 V, the gate voltage at 50 V, and the drain voltage at −60 V indicates a drift of the not immobilized dopants out of the OFET channel resulting in changed electronic properties of the film and nonstable device behavior.

voltage regime and in the backward direction toward the negative. This shift can be explained with the drift of the mobile dopants within the active layer of the device. Starting measurement in the off-state of the transistor at a gate voltage of 50 V with the source contact at 0 V and the drain contact at −60 V, the positively charged mobile dopant ions are driven away from the gate and hence also the conductive channel of the OFET (Figure 5c). Due to the three terminal device architecture with overlaying source–drain, source–gate, and also drain–gate fields, the dopant drift is probably not directed perpendicular away from the gate, but in this situation rather diagonal toward the drain contact at −60 V. In any case, the dopant depletion in the channel should result in less compensation doping in this important device region and therefore in higher drain currents eventually, which reflects in the earlier onset of the transistors. Equivalent mechanisms hold for the threshold voltage shift in the backward direction.

The assumption of the dopant drift influencing the electronic properties of the OFETs is supported by several additional indicators. First, increasing the measurement range of the gate voltage from 50 to 100 V leads to stronger hysteresis for nonimmobilized dopants. Also for the case of 10 mol% of UV activated o-AzBnO-DMBI hysteresis is then visible to a lesser extent, which is in line with the suspicion that charged dopant agglomerates can potentially drift within the thin film. However, for a ratio of 0.1 mol% UV activated o-AzBnO-DMBI resulting in the highest field-effect mobilities overall no hysteresis is found even after measuring in the extended gate voltage range (Figure S7, Supporting Information). Instead of increasing the measurement range, it is furthermore possible to write and read the devices like Lee et al. have done. Applying a gate voltage of ±100 V for 10 s leads to reproducible threshold voltage shifts of the devices with nonimmobilized dopants, which can then be read out in transfer curve measurements

(Figure S8, Supporting Information). A final further indicator is that increasing the amount of the not immobilizable o-BnO-DMBI in OFETs also results in increasing hysteresis besides decreased off-currents through the n-doping effect (Figure S9, Supporting Information).

In summary, we have found a traceable way to control dopant drift in organic semiconductor films, which has a great impact on device performance. Comparing the two n-dopants o-BnO-DMBI and the azide-functionalized and thus immobilizable o-AzBnO-DMBI, we first showed that both similarly compensate oxygen doping in P3HT. Immobilization of the latter in the P3HT matrix took place after nitrene generation through UV activation and could inhibit the negative side effects of mobile ions in OFETs. Devices with the immobilized o-AzBnO-DMBI show two orders of magnitude larger on/off-ratios than simple P3HT OFETs, but similar field-effect mobilities and no amplified hysteresis due to successful prevention of the dopant drift. This approach is a powerful and promising tool to solve the problem of air instability of P3HT regarding oxygen doping and hysteresis effects, hopefully making this widely used polymer more attractive for OFET mass fabrication. Thanks to the nonspecific character of the binding process between o-AzBnO-DMBI and host molecule, our goal will now be to expand and apply our immobilization strategy to other p-type semiconductors of interest and to expand it toward p-type organic dopants.

3. Experimental Section

Materials: P3HT (M_w = 26 623 g mol^{-1}, regioregularity = 96.7%, polydispersity = 1.75) from BASF SE was used as received without further purification. o-BnO-DMBI and o-AzBnO-DMBI were synthesized and purified as published elsewhere.[46]

Sample Fabrication: Materials were dissolved separately in chlorobenzene. P3HT was stirred at 50 °C over several hours. Dopants

**ADVANCED
SCIENCE NEWS**

www.advancedsciencenews.com

**ADVANCED
MATERIALS
TECHNOLOGIES**

www.advmattechnol.de

were dissolved for ≈15 min. Solutions were then mixed with several different molar ratios of dopant to P3HT. Total mass content for OFET fabrication was 10 g L^{-1} giving film thicknesses around 50 nm. For IR, XPS, UV–vis, SEM, and TEM measurements, mass content was 7.5 g L^{-1} leading to around 30 nm. Films were spin coated in air at 1000 RPM for 60 s with an acceleration of 500 RPM s^{-1} on glass substrates (Borofloat 33, Schott) with thermally evaporated gold contacts for *IV*-measurements. The thickness of the contacts was 60 nm, and channel length and width were 20 µm and 1 mm, respectively. For IR and SEM, silicon substrates were used, for XPS, indium tin oxide (ITO) substrates, and for UV–vis, quartz-glass. For TEM measurements, glass substrates were treated with O$_2$-plasma for 5 min, before poly(3,4-ethylenedioxythiophene) polystyrene sulfonate (PEDOT:PSS) (Heraeus Clevios) filtered through 0.45 µm PTFE-filters was spin coated on them with a 2-step process. First 1000 RPM for 10 s with an acceleration of 4300 RPM s^{-1} were used, which was followed by a second step with 4300 RPM for 30 s with 4300 RPM s^{-1} giving roughly 40 nm. The PEDOT:PSS was then heated at 130 °C for 30 min, and before doped P3HT films were spin coated on top as described above. Through depositing samples in deionized water, the films could then be transferred on TEM-grids for measurements. Activation by UV light was performed using a mercury-vapor lamp GPH135T5L/4 from Peschl UV-products. The lamp has a nominal UV-C power of 1.2 W at 254 nm and was placed 10 cm above the samples. For OFETs, ≈500 nm poly(chloro-*p*-xylylene) (Parylene C) was deposited on top of the active layer as a dielectric via chemical vapor deposition in a commercially available PDS2010 coating system by Specialty Coating Systems, before silver gate contacts were thermally evaporated.

Electrical Measurements: All electrical measurements were performed in air at room temperature and in the dark using a Semiconductor Parameter Analyzer 4155C by Agilent Technologies. Several samples were fabricated and representative measurements were shown. For statistics, always at least three different samples were considered providing standard deviation as statistical error. Conductivities were calculated from *IV*-measurements on the corresponding films used in OFETs. OFET transfer characteristics were measured by device operation in accumulation mode. Field-effect mobilities in the saturated regime were then calculated from the transconductance according to the formula

$$\mu_{sat} = \left(\frac{2L}{WC}\right)\left(\frac{\partial\sqrt{I_D}}{\partial V_G}|_{v_o = const.}\right)^2$$

as described elsewhere.[50] Threshold voltages were evaluated through the intersection of the extrapolation of $\sqrt{I_D}$ in the saturation region with the axis of abscissae as described elsewhere as well.[51]

UV–Vis spectroscopy: UV–vis spectroscopy was performed using a Jasco UV/VIS V-670 spectrophotometer.

Scanning Electron Microscopy: SEM images were taken with a modular crossbeam workstation of the AURIGA series by Carl Zeiss NTS GmbH operated at 1 kV.

Transmission Electron Microscopy: EELS and ESI measurements were performed using a Libra 200 MC (Carl Zeiss Microscopy GmbH, Germany) operated at 60 kV equipped with combination of a monochromator, an in-column energy-filter, and Cs-Corrector (CEOS GmbH, Germany) providing high spatial and energy resolution. EEL spectra were recorded from pure layers of P3HT, *o*-BnO-DMBI, and *o*-AzBnO-DMBI at an energy resolution of 100 meV. Conventional TEM images and ESI images at 6.5 eV energy-loss were acquired from blends of P3HT layers doped with *o*-BnO-DMBI or *o*-AzBnO-DMBI. To record ESI images, an energy-selecting slit was needed to be inserted into the dispersive plane. The slit width was set to 1 eV to ensure that only electrons contribute to the ESI image that induced plasmon excitations. The pixel sizes of conventional TEM and ESI raw images were 0.2 and 0.5 nm, respectively. ESI images were processed using a threshold filter for removing outlying pixels and 2 × 2 binning. For enhancing the contrast of the dopant agglomerates, the ESI images at 6.5 eV were normalized with regard to the remaining mass thickness contrast with the corresponding 2 × 2 binned TEM image. For the first image at 6.5 eV, a dose of 144 eÅ^{-2} was applied. For the second ESI image at the same sample area, a dose of 451 eÅ^{-2} was applied, after which the contrast of the dopant agglomerates disappeared due to irradiation damage.

Infrared Spectroscopy: IR measurements were carried out with the Fourier-transform IR spectrometer Vertex 80 (Bruker). The spectrometer with the sample was under vacuum (3 mbar) to clear the spectra from absorption lines of air, mainly H$_2$O and CO$_2$. Each spectrum was recorded for almost normal transmittance (7°) with an MCT detector and had a resolution of 4 cm^{-1}. One spectrum consists of the average of 200 scans.

Photoelectron Spectroscopy: Photoelectron spectroscopy data were recorded using a PHI5000 VersaProbe scanning photoelectron spectrometer equipped with a monochromated Al Kα X-ray source (1486.7 eV) and a differentially pumped helium discharge lamp (21.2 eV).

Supporting Information

Supporting Information is available from the Wiley Online Library or from the author.

Acknowledgements

Conflict of Interest

The authors declare no conflict of interest.

Keywords

[1] M. T. Dang, L. Hirsch, G. Wantz, *Adv. Mater.* **2011**, *23*, 3597.

[2] G. Dennler, M. C. Scharber, C. J. Brabec, *Adv. Mater.* **2009**, *21*, 1323.

[3] G. Li, R. Zhu, Y. Yang, *Nat. Photonics* **2012**, *6*, 153.

[4] S. Holliday, R. S. Ashraf, A. Wadsworth, D. Baran, S. A. Yousaf, C. B. Nielsen, C.-H. Tan, S. D. Dimitrov, Z. Shang, N. Gasparini, M. Alamoudi, F. Laquai, C. J. Brabec, A. Salleo, J. R. Durrant, I. Mcculloch, *Nat. Commun.* **2016**, *7*, 11585.

[5] A. Kumar, J. Hasan, A. Majji, A. Avhale, S. Gopinathan, P. Sharma, D. Tarange, R. Bajpai, A. Kumar, *J. Flow Chem.* **2014**, *4*, 206.

[6] R. H. Lohwasser, M. Thelakkat, *Macromolecules* **2011**, *44*, 3388.

[7] P. Kohn, S. Huettner, H. Komber, V. Senkovskyy, R. Tkachov, A. Kiriy, R. H. Friend, U. Steiner, W. T. S. Huck, J.-U. Sommer, M. Sommer, *J. Am. Chem. Soc.* **2012**, *134*, 4790.

[8] P. Apilo, M. Välimäki, R. Po, K.-L. Väisänen, H. Richter, M. Ylikunnari, M. Vilkman, A. Bernardi, G. Corso, H. Hoppe, R. Roesch, R. Meitzner, U. S. Schubert, J. Hast, *Sol. RRL* **2018**, *2*, 1700160.

[9] M. Manceau, D. Angmo, M. Jørgensen, F. C. Krebs, *Org. Electron.* **2011**, *12*, 566.

[10] R. R. Søndergaard, M. Hösel, F. C. Krebs, *J. Polym. Sci., Part B: Polym. Phys.* **2013**, *51*, 16.

[11] M. S. A. Abdou, F. P. Orfino, Y. Son, S. Holdcroft, *J. Am. Chem. Soc.* **1997**, *119*, 4518.

[12] H.-H. Liao, C.-M. Yang, C.-C. Liu, S.-F. Horng, H.-F. Meng, J.-T. Shy, *J. Appl. Phys.* **2008**, *103*, 104506.

[13] C.-K. Lu, H.-F. Meng, *Phys. Rev. B* **2007**, *75*, 235206.

[14] E. J. Meijer, C. Detcheverry, P. J. Baesjou, E. Van Veenendaal, D. M. De Leeuw, T. M. Klapwijk, *J. Appl. Phys.* **2003**, *93*, 4831.

[15] W.-Y. Lee, H.-C. Wu, C. Lu, B. D. Naab, W.-C. Chen, Z. Bao, *Adv. Mater.* **2017**, *29*, 1605166.

[16] S. M. Sze, K. K. Ng, *Physics of Semiconductor Devices*, John Wiley & Sons, Inc., Hoboken, NJ **2006**.

[17] S. O. Kasap, *Principles of Electronic Materials and Devices*, McGraw-Hill, New York **2006**.

[18] H. Fujii, Y. Wang, K. Watanabe, M. Sugiyama, Y. Nakano, *J. Appl. Phys.* **2013**, *114*, 103101.

[19] S. B. Zhang, *J. Phys.: Condens. Matter* **2002**, *14*, R881.

[20] J. Zhang, K. Tse, M. Wong, Y. Zhang, J. Zhu, *Front. Phys.* **2016**, *11*, 117405.

[21] S. Hunklinger, *Festkörperphysik*, De Gruyter Oldenbourg, Munich **2014**.

[22] M. Rudan, *Physics of Semiconductor Devices*, Springer, New York **2015**.

[23] I. Salzmann, G. Heimel, *J. Electron Spectrosc. Relat. Phenom.* **2015**, *204*, 208.

[24] I. E. Jacobs, A. J. Moulé, *Adv. Mater.* **2017**, *29*, 1703063.

[25] G. Lu, J. Blakesley, S. Himmelberger, P. Pingel, J. Frisch, I. Lieberwirth, I. Salzmann, M. Oehzelt, R. Di Pietro, A. Salleo, N. Koch, D. Neher, *Nat. Commun.* **2013**, *4*, 1588.

[26] N. Stingelin-Stutzmann, E. Smits, H. Wondergem, C. Tanase, P. Blom, P. Smith, D. De Leeuw, *Nat. Mater.* **2005**, *4*, 601.

[27] J. Smith, R. Hamilton, I. Mcculloch, N. Stingelin-Stutzmann, M. Heeney, D. D. C. Bradley, T. D. Anthopoulos, *J. Mater. Chem.* **2010**, *20*, 2562.

[28] J. Smith, R. Hamilton, Y. Qi, A. Kahn, D. D. C. Bradley, M. Heeney, I. Mcculloch, T. D. Anthopoulos, *Adv. Funct. Mater.* **2010**, *20*, 2330.

[29] L. Müller, S.-Y. Rhim, V. Sivanesan, D. Wang, S. Hietzschold, P. Reiser, E. Mankel, S. Beck, S. Barlow, S. R. Marder, A. Pucci, W. Kowalsky, R. Lovrincic, *Adv. Mater.* **2017**, *29*, 1701466.

[30] A. Dai, A. Wan, C. Magee, Y. Zhang, S. Barlow, S. R. Marder, A. Kahn, *Org. Electron.* **2015**, *23*, 151.

[31] T.-D. Tsai, J.-W. Chang, T.-C. Wen, T.-F. Guo, *Adv. Funct. Mater.* **2013**, *23*, 4206.

[32] S. Zhu, G. Zhou, W. Yuan, S. Mao, F. Yang, G. Fu, B. Sun, *J. Colloid Interface Sci.* **2020**, *560*, 565.

[33] J. Jang, S. H. Kim, S. Nam, D. S. Chung, C. Yang, W. M. Yun, C. E. Park, J. B. Koo, *Appl. Phys. Lett.* **2008**, *92*, 143306.

[34] S. Kobayashi, T. Nishikawa, T. Takenobu, S. Mori, T. Shimoda, T. Mitani, H. Shimotani, N. Yoshimoto, S. Ogawa, Y. Iwasa, *Nat. Mater.* **2004**, *3*, 317.

[35] S. Duhm, I. Salzmann, G. Bröker, H. Glowatzki, R. L. Johnson, N. Koch, *Appl. Phys. Lett.* **2009**, *95*, 093305.

[36] Y. Xu, H. Sun, A. Liu, H.-H. Zhu, W. Li, Y.-F. Lin, Y.-Y. Noh, *Adv. Mater.* **2018**, *30*, 1801830.

[37] J. Li, C. W. Rochester, I. E. Jacobs, S. Friedrich, P. Stroeve, M. Riede, A. J. Moulé, *ACS Appl. Mater. Interfaces* **2015**, *7*, 28420.

[38] B. D. Naab, S. Zhang, K. Vandewal, A. Salleo, S. Barlow, S. R. Marder, Z. Bao, *Adv. Mater.* **2014**, *26*, 4268.

[39] B. D. Naab, S. Guo, S. Olthof, E. G. B. Evans, P. Wei, G. L. Millhauser, A. Kahn, S. Barlow, S. R. Marder, Z. Bao, *J. Am. Chem. Soc.* **2013**, *135*, 15018.

[40] P. Wei, J. H. Oh, G. Dong, Z. Bao, *J. Am. Chem. Soc.* **2010**, *132*, 8852.

[41] G. Kwon, K. Kim, B. D. Choi, J. Roh, C. Lee, Y.-Y. Noh, S. Seo, M.-G. Kim, C. Kim, *Adv. Mater.* **2017**, *29*, 1607055.

[42] S. Rossbauer, C. Müller, T. D. Anthopoulos, *Adv. Funct. Mater.* **2014**, *24*, 7116.

[43] J. Liu, L. Qiu, G. Portale, M. Koopmans, G. Ten Brink, J. C. Hummelen, L. J. A. Koster, *Adv. Mater.* **2017**, *29*, 1701641.

[44] D. Kiefer, A. Giovannitti, H. Sun, T. Biskup, A. Hofmann, M. Koopmans, C. Cendra, S. Weber, L. J. Anton Koster, E. Olsson, J. Rivnay, S. Fabiano, I. Mcculloch, C. Müller, *ACS Energy Lett.* **2018**, *3*, 278.

[45] X.-Q. Zhu, M.-T. Zhang, A. Yu, C.-H. Wang, J.-P. Cheng, *J. Am. Chem. Soc.* **2008**, *130*, 2501.

[46] P. Reiser, F. S. Benneckendorf, M.-M. Barf, L. Müller, R. Bäuerle, S. Hillebrandt, S. Beck, R. Lovrincic, E. Mankel, J. Freudenberg, D. Jänsch, W. Kowalsky, A. Pucci, W. Jaegermann, U. H. F. Bunz, K. Müllen, *Chem. Mater.* **2019**, *31*, 4213.

[47] M. Pfannmöller, H. Flügge, G. Benner, I. Wacker, C. Sommer, M. Hanselmann, S. Schmale, H. Schmidt, F. A. Hamprecht, T. Rabe, W. Kowalsky, R. R. Schröder, *Nano Lett.* **2011**, *11*, 3099.

[48] B. Lüssem, M. L. Tietze, H. Kleemann, C. Hoßbach, J. W. Bartha, A. Zakhidov, K. Leo, *Nat. Commun.* **2013**, *4*, 2775.

[49] S. Olthof, S. Singh, S. K. Mohapatra, S. Barlow, S. R. Marder, B. Kippelen, A. Kahn, *Appl. Phys. Lett.* **2012**, *101*, 253303.

[50] D. Choi, P.-H. Chu, E. McBride, E. Reichmanis, *Chem. Mater.* **2015**, *27*, 4167.

[51] C. Bock, D. V. Pham, U. Kunze, D. Käfer, G. Witte, C. Wöll, *J. Appl. Phys.* **2006**, *100*, 114517.